JOURNAL OF APPLIED POLYMER SCIENCE VOL. 16, PP. 275-299 (1972)

Relationship in Polypropylene Melt Between Its Linear Viscoelasticity and Its Steady Capillary Flow Properties

MITSUYOSHI FUJIYAMA and HIROSHI AWAYA, *Research Laboratory, Tokuyama Soda Co., Ltd., Tokuyama-shi, Yaguchi-ken, Japan*

Synopsis

It is the object of the present study to obtain clear knowledge of the relations in the polypropylene melt between its linear viscoelasticity and its nonlinear steady capillary flow, paying particular attention to the elastic properties in its capillary flow. By representing the linear viscoelasticity numerically with zero-shear viscosity, η_0, and steady-state compliance, J_e^0, evaluation has been made of the properties concerning the elasticity of polymer melt in the capillary flow, such as non-Newtonianity, the entrance pressure loss, the end correction, the Barus effect, and the melt fracture. The steady flow viscosity η, the entrance pressure loss P_0, the critical shear stress, τ_c, and the critical shear rate $\dot{\gamma}_c$ at which melt fracture begins to occur are subject to η_0 as follows:

$$\log \eta \propto \log \eta_0, \log P_0 \propto \log \eta_0, \tau_c \propto -\log \eta_0, \log \dot{\gamma}_c \propto -\log \eta_0.$$

From the well-known relationship between η_0 and the weight-average molecular weight $\bar{M}_w$, these quantities are governed by $\bar{M}_w$. Meanwhile, for such quantities as structural viscosity index N, end correction coefficient ν, and elastic pressure loss ratio P_0/P, following correlations hold:

$$N \propto \log (\eta_0 \cdot J_e^0), \log \nu \propto \log (\eta_0^2 \cdot J_e^0), P_0/P \propto \log (\eta_0^2 \cdot J_e^0).$$

As η_0 and J_e^0 are respectively determined mainly by $\bar{M}_w$ and the molecular weight distribution MWD, these quantities are governed by both $\bar{M}_w$ and MWD. Physical meanings of $\eta_0 \cdot J_e^0$ and $\eta_0^2 \cdot J_e^0$ are, respectively, mean relaxation time and a measure of stored energy in steady flow. The Barus effect has a positive correlation to J_e^0, ν, and P_0/P. (The symbol $\propto$ employed here means positive correlation.)

INTRODUCTION

Polymeric materials are usually processed to various shaped articles via the easily deformable molten state. Consequently, the flow of the molten polymer is the most basic phenomenon in the processing of polymeric materials, and it is not an exaggeration to say that the flow properties are directly related to processability. The flow properties of polymeric materials are measured by various types of rheometers, such as a capillary viscometer, a rotational viscometer, etc. A capillary viscometer is most practical for the evaluation of the processability on a laboratory scale.

The actual processing is performed in a large deformation region where nonlinear viscoelasticity plays an important role. However, a nonlinear

viscoelasticity theory has not been established, even phenomenologically. On the other hand, linear viscoelasticity can be fairly well described by molecular theory. If the relation between linear viscoelasticity and capillary flow properties, which are measures for the actual processability, could be established, it would be possible to evaluate processability by means of molecular theory and to realize molecular design about processability. This has so far been a goal of polymer physicists.

The relations between linear viscoelasticity and nonlinear steady flow properties were derived by means of the continuum theory by Coleman-Markovitz,[1] Pao[2-4] and Huseby-Blyler,[5] but the theories presented did not fit the experimental results well. On the other hand, Cox-Merz[6-8] and Onogi et al.[9] have experimentally found that the apparent viscosity $\eta_a(\dot{\gamma})$ coincided with the absolute value of the complex viscosity $|\eta^*(\omega)|$. La Nieve and Bogue[30] have correlated the elastic pressure drop ΔP_E from capillary experiments with the normal stress difference $T_{11} - T_{22}$ from an independent measurement. There have so far been no investigations to study the relations between elastic properties in capillary flow and linear viscoelasticity.

Now, a polymer melt shows viscosity and elasticity and behaves viscoelastically when it is deformed. In some past investigations about processability, the polymer melt was regarded as a fluid with viscosity only, but without elasticity. The elasticity of the polymer melt must never be disregarded since it manifests itself as various phenomena in the actual processing. For example, in blow molding or in vacuum forming, elasticity allows the molten polymer to hold its shape before being formed. The lack of elasticity permits flow, and irregularly shaped parts result. Too much elasticity may lead to excess "swell" in blow molding, and the formed part will be thicker and heavier than designed. In injection molding, too much elasticity causes frozen stress. In extrusion molding, the elasticity is a cause of pressure loss at die inlet and participates in the occurrence of melt fracture.

The purpose of this study is to obtain experimentally the relations between linear viscoelasticity and nonlinear steady-flow properties, especially the elastic properties of polypropylene melt in capillary flow.

EXPERIMENTAL

Materials

The samples used are shown in Table I. They were commercial isotactic polypropylenes with melt flow indexes of 0.6–11.4. The viscosity-average molecular weight $\bar{M}_v$ was determined from the intrinsic viscosity $[\eta]$ in tetralin at 135°C using Parrini's equation[10]:

$$[\eta] = 0.80 \times 10^{-4} \bar{M}_w^{0.80} \tag{1}$$

Linear Viscoelasticity

Linear viscoelasticity of the polypropylene melt was measured with a plate relaxometer recently constructed by Takayanagi and his co-workers.[11]

TABLE I
Properties of Polypropylene Samples

Sample	M.I., dg/min	$\bar{M}_v \times 10^{-5}$	η_{0p}, poises	J_e^0, cm²/dyne	ΔH_a, kcal/mole
A-1	0.6	4.1	5.46×10^5	2.64×10^{-5}	9.7
B-1	0.7	4.0	5.57×10^5	3.88×10^{-4}	9.5
C-1	0.8	4.2	4.20×10^5	1.38×10^{-4}	8.7
A-2	3.6	2.3	1.22×10^5	2.94×10^{-5}	8.3
B-2	3.7	2.8	1.41×10^5	3.07×10^{-4}	9.5
A-3	4.2	2.8	1.22×10^5	1.93×10^{-4}	10.2
B-3	5.6	2.4	7.99×10^4	4.01×10^{-4}	9.5
C-2	6.8	2.5	6.23×10^4	1.26×10^{-4}	9.9
A-4	11.4	2.2	3.83×10^4	2.64×10^{-4}	10.0

The principle of the measurement is shown in Figure 1. A rectangular plate is inserted into the center of a box-shaped cell filled with polymer melt along the cell wall and fixed at the desired position. The cell is instantaneously shifted down along the plane of the plate by a definite displacement, and the force generated on the plate is measured as a function of time.

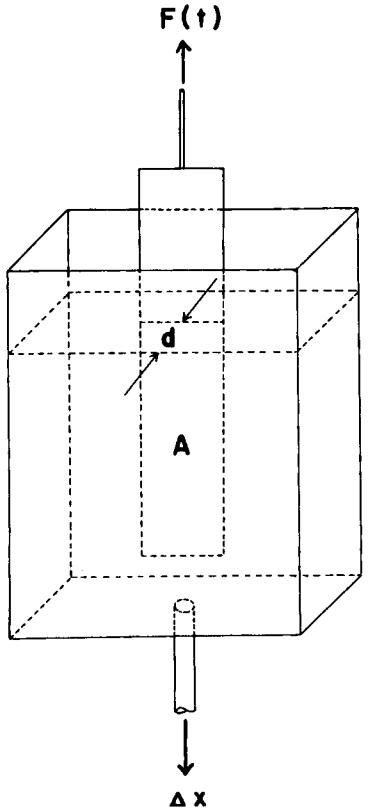

Fig. 1. Principle of plate relaxometer.

The shift given to the cell is observed with a dial gauge, and the force generated on the plate is detected by a strain gauge. Shear relaxation modulus $G(t)$ is calculated from the following equation:

$$G(t) = \frac{\frac{F(t)}{2A}}{\frac{\Delta x}{d}} \tag{2}$$

where $F(t)$ is the force generated on the plate, Δx is the displacement given to the cell, A is the area of one side of the plane of the plate immersed in the sample, and d is the distance between the plane of the plate and the cell wall.

Shear relaxation modulus $G(t)$ was measured at 170–250°C, and a master curve based on 230°C was obtained according to the time–temperature superposition principle.[12]

The zero-shear viscosity η_0 and the steady-state compliance J_e^0 are calculated from $G(t)$ by the eqs. (3) and (4), respectively[12]:

$$\eta_0 = \int_0^\infty G(t)dt \tag{3}$$

$$J_e^0 = \frac{\int_0^\infty t \cdot G(t)dt}{\eta_0^2} \tag{4}$$

It can be seen from eqs. (3) and (4) that the values of η_0 and J_e^0 are determined mainly by the position and the shape of the relaxation modulus curve, respectively. Consequently, η_0 and J_e^0 can be regarded as the numerical measures of the relaxation modulus curve. According to the theory of linear viscoelasticity, if one kind of viscoelastic function (relaxation modulus in this case) is known, any kind of viscoelastic function can be calculated by a mathematical transformation. Hence, η_0 and J_e^0 can be also regarded as the numerical measures of the linear viscoelasticity. From the reason mentioned above, η_0 and J_e^0 were used as the measure of linear viscoelasticity in order to investigate the relations between linear viscoelasticity and steady capillary flow properties.

TABLE II
Dimensions of Dies

No.	Diameter $2R$, mm	Length L, mm	L/R
1	0.5	1.0	4
2	0.5	2.0	8
3	0.5	2.5	10
4	0.5	3.5	14
5	0.5	5.0	20

Steady Capillary Flow Properties

Steady capillary flow properties were measured at 230°C with a Koka flow tester, a plunger extrusion-type rheometer produced by the Shimazu Seisakusho Co. Ltd., Japan. The dimensions of the dies used are shown in Table II. The taper angles of all dies were 90°.

In the case of steady capillary flow of a Newtonian fluid, the shear stress τ_w' and the shear rate, $\dot{\gamma}_w'$ at the wall of the capillary are given by eqs. (5) and (6), respectively:

$$\tau_w' = \frac{PR}{2L} \tag{5}$$

$$\dot{\gamma}_w' = \frac{4Q}{\pi R^3} \tag{6}$$

where R and L are radius and length of the capillary, respectively, Q is the volumetric output rate of the fluid, and P is the applied pressure.

In the case of the Koka flow tester, in which fluid flows from the reservoir with a relatively large diameter into the die with a relatively small diameter, pressure loss due to the contraction of the flow at the die inlet, P_c, occurs. In such cases, τ_w' in eq. (5) is an apparent shear stress, and the effective shear stress τ_w'' is given by the following equations:

$$\tau_w'' = (P - P_c)\frac{R}{2L} \tag{7}$$

$$= \frac{PR}{2(L + n_cR)} \tag{8}$$

where n_cR is the capillary length corresponding to P_c; n_c is known as Couette's correction term coefficient, and its value is 0.77.[13]

When a fluid is a viscoelastic material such as a polymer melt, the pressure loss due to the elastic deformation at the die inlet, P_e, must be also considered, and the effective shear stress τ is given as follows:

$$\tau = (P - P_c - P_e)\frac{R}{2L} \tag{8}$$

$$= (P - P_0)\frac{R}{2L} \tag{8'}$$

$$= \frac{PR}{2(L + n_cR + SR)} \tag{8''}$$

$$= \frac{PR}{2(L + \nu R)} \tag{8'''}$$

$$P_0 = \frac{P(n_cR + SR)}{(L + n_cR + SR)} \tag{9}$$

$$= \frac{PR}{(L + \nu R)} \tag{9'}$$

and

$$P_0 = P_c + P_e \tag{10}$$

$$\nu = n_c + S \tag{11}$$

where SR is the capillary length corresponding to P_e.

When flow is non-Newtonian, a correction is needed for the shear rate. The true shear rate $\dot{\gamma}$ is given by eq. (12):

$$\dot{\gamma} = \frac{1}{4}\left\{3 + \frac{d \log \dot{\gamma}_w'}{d \log \tau}\right\} \dot{\gamma}_w'. \tag{12}$$

When $\dot{\gamma}_w'$ and τ are correlated by the so-called power law,

$$\dot{\gamma}_w' = K\tau^N \tag{13}$$

where K and N are constants, eq. (12) can be rewritten as follows:

$$\dot{\gamma} = (3 + N)\frac{\dot{\gamma}_w'}{4}. \tag{14}$$

N is called the power law index.

The non-Newtonian flow curve could not be quantitatively determined from the measurement with the aid of a capillary viscometer without correction based on the eqs. (8) and (12). Furthermore, apparent viscosity η is given by

$$\eta = \frac{\tau}{\dot{\gamma}}. \tag{15}$$

RESULTS AND DISCUSSION

Linear Viscoelasticity

An example of the shear relaxation modulus $G(t)$, measured with the plate relaxometer at various temperatures, is shown in Figure 2. The higher the temperature, the longer the time of the relaxation modulus curve. It is seen that all relaxation modulus curves are superposable by shifting them along the time axis. The master curve for relaxation modulus obtained by shifting all relaxation modulus curves to the 230°C curve is shown in Figure 3. The master relaxation modulus curves of all samples are shown in Figure 4. The position and the shape of the curve vary with every sample.

Zero-shear viscosity η_{0p} and steady-state shear compliance J_e^0, calculated by means of graphical integration according to the eqs. (3) and (4), are shown in Table I. The subscript p in η_{0p} means that η_{0p} was measured with a plate relaxometer. The η_{0p} value ranged from 3.83×10^4 to 5.57×10^5 poises, and J_e^0, was from 2.64×10^{-5} to 4.01×10^{-4} cm²/dyne.

The correlation between η_{0p} and the viscosity-average molecular weight $\bar{M}_v$ is shown in Figure 5. η_{0p} was proportional to $\bar{M}_v^{4.0}$, which was a little stronger molecular weight dependence than the 3.4 power law.

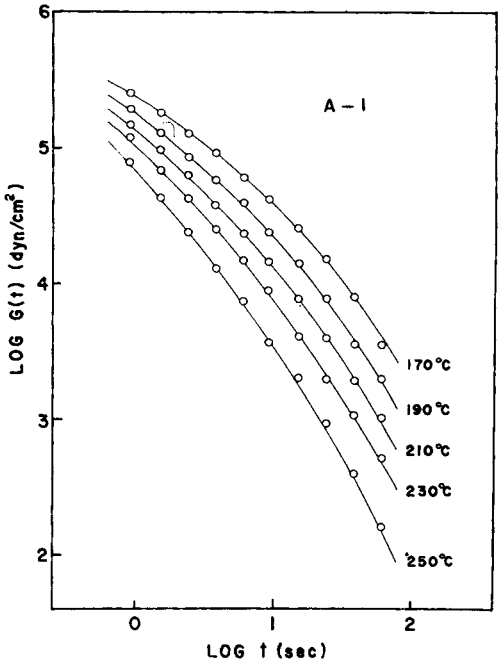

Fig. 2. Temperature variation of shear relaxation modulus $G(t)$ for sample A-1.

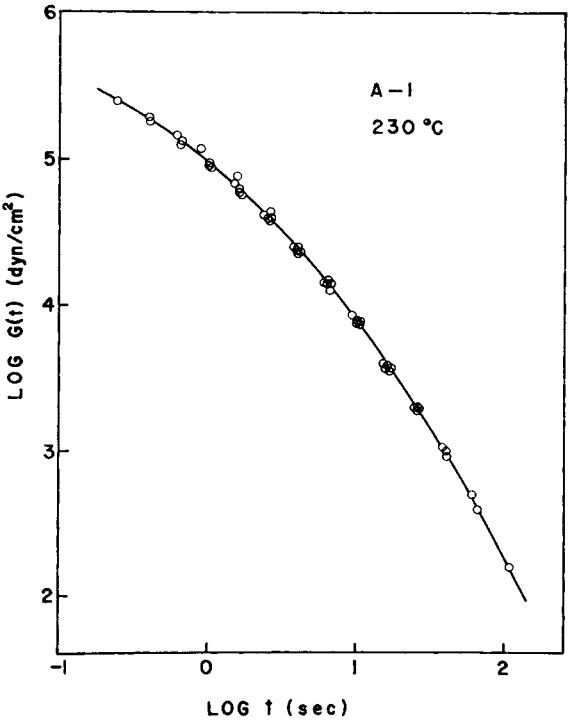

Fig. 3. Master curve of shear relaxation modulus for sample A-1.

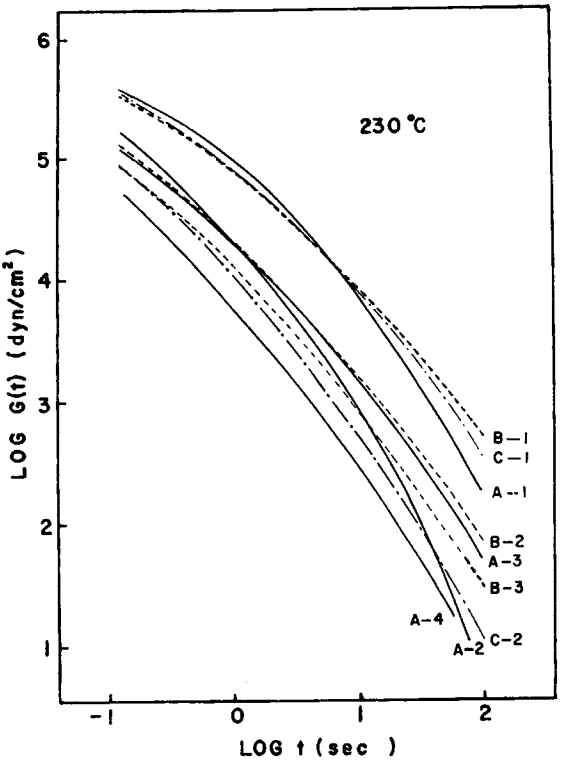

Fig. 4. Master curves of shear relaxation modulus for all samples.

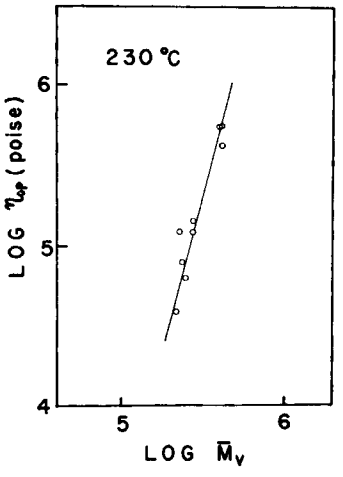

Fig. 5. Dependence of zero-shear viscosity, η_{0p} on viscosity-average molecular weight $\bar{M}v$.

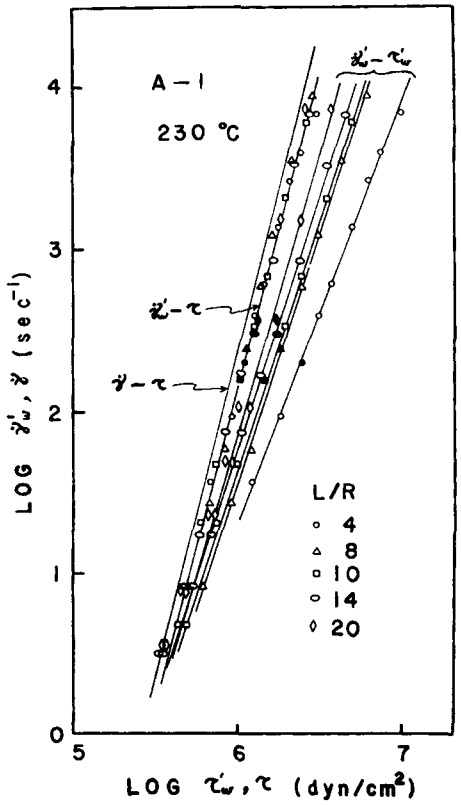

Fig. 6. Flow curves for sample A-1 corrected at each stage.

If the logarithm of shift factor a_T, which is the horizontal shift when obtaining the master relaxation modulus curve according to the time–temperature superposition principle, was plotted against the reciprocal of absolute temperature T, a linear relationship was obtained, and the following equation could be applied:

$$a_T = A \exp (\Delta H_a/RT) \tag{16}$$

where A is a constant independent of temperature, ΔH_a is the apparent activation energy of relaxation, and R is the gas constant. The value of ΔH_a obtained from the slope of the line is shown in Table I. The value of ΔH_a of isotactic polypropylene was about 10 kcal/mole.

Steady Capillary Flow Properties

End Correction

An example of the apparent flow curves in the form of $\dot{\gamma}_w'$ versus τ_w', calculated from P and Q using eqs. (5) and (6), are shown in Figure 6. The smaller the L/R of die was, the more the apparent flow curve shifted to the higher shear stress and the easier the slope of the curve was. If there was

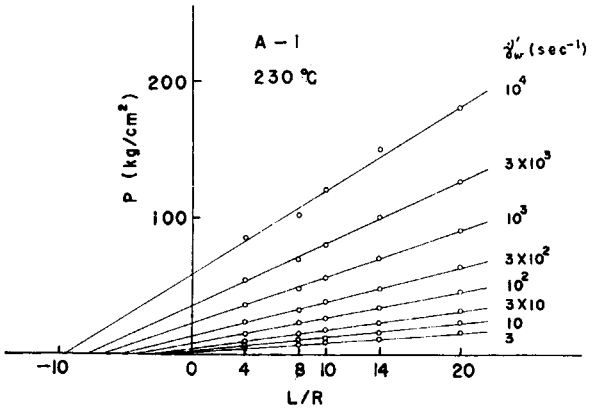

Fig. 7. Bagley plot.

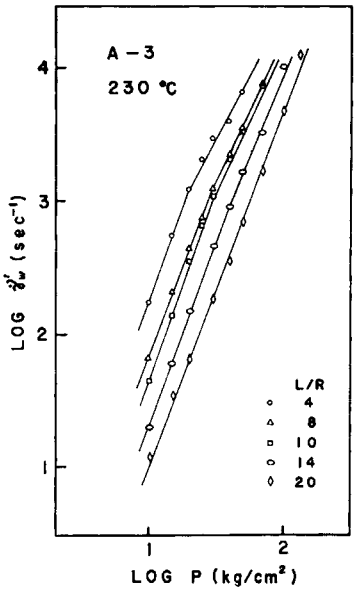

Fig. 8. Relations between apparent shear rate $\dot{\gamma}_w'$ and pressure P.

no pressure loss at the die inlet, all apparent flow curves in Figure 6 should be combined into one flow curve.

Now eqs. (8′) and (8‴) can be rearranged to the eqs. (17) and (18):

$$P = 2\tau(L/R) + P_0 \tag{17}$$

$$P = 2\tau(L/R) + 2\nu\tau \tag{18}$$

Thus, if the pressure loss P required to produce a definite shear rate $\dot{\gamma}_w'$ is plotted against L/R, a linear relationship must be obtained. Apparently from eqs. (17) and (18), the intercept of the P axis is P_0, and the intercept of the L/R axis is $-\nu$. This procedure is called the Bagley plot. Using the

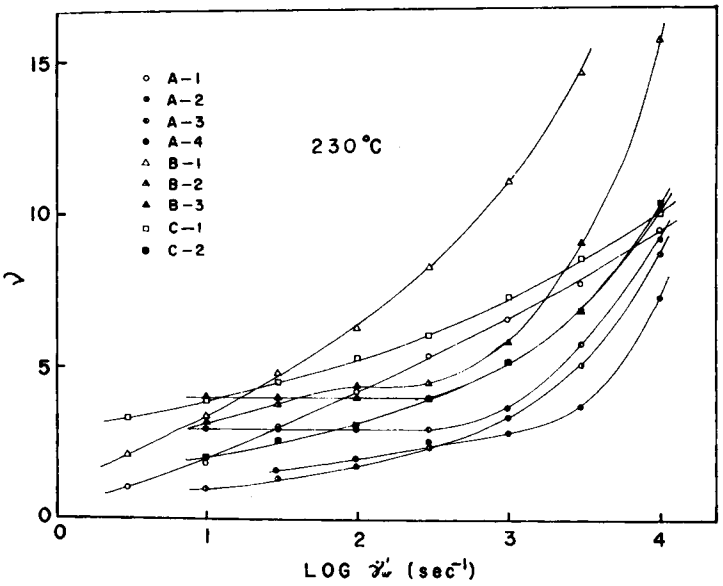

Fig. 9. Shear rate variation of end correction coefficient ν.

apparent flow curves in the form of $\dot{\gamma}_w'$ versus P, rewritten from the apparent flow curves in the form of $\dot{\gamma}_w'$ versus τ_w' in Figure 6, a Bagley plot is shown in Figure 7. Fairly good linear relationships were obtained for all samples. The apparent flow curves of the samples whose melt indexes (M.I.) are higher than that of A-2 sample have "creases" at the shear rate of about 10^3 sec^{-1}. Such a case is shown for the A-3 sample in Figure 8. The smaller the L/R of the die, the stronger the degree of creasing. Since the lower limit of applied pressure in the Koka flow tester is 10 kg/cm^2, the

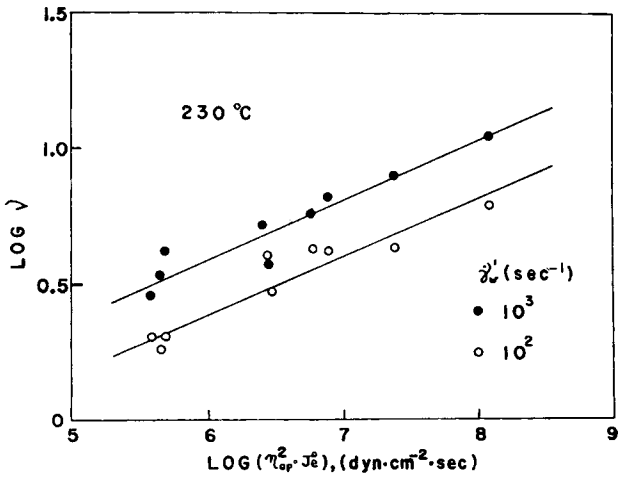

Fig. 10. Relation betwen ν and $\eta^2_{0p}\cdot J_e^0$.

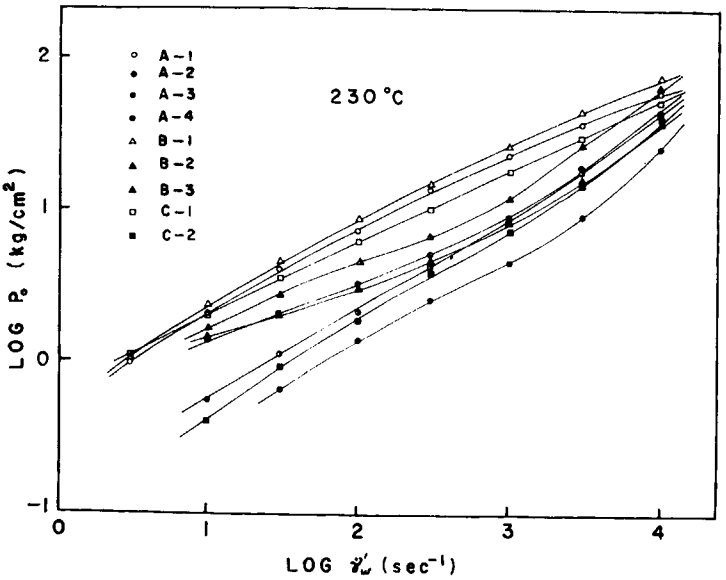

Fig. 11. Shear rate variation of entrance pressure loss P_e.

measurable shear rate has also a lower limit. This lower limit is serious when a sample of high melt index is tested with a die of small L/R value. In such a case, a Bagley plot for the shear rate lower than the limit was done by extrapolation.

The Bagley plot was applied for all samples, and the end correction coefficient ν was obtained as a function of apparent shear rate $\dot{\gamma}_w'$ as shown in Figure 9. The relations of ν versus log $\dot{\gamma}_w'$ curved upward. These results disagree with the results Kamide et al.,[17,18] in which linear relations were obtained for polypropylene melts.

As the end correction coefficient ν is a measure of the elasticity of polymer melt flowing in a capillary and the steady-state compliance J_e^0 is a measure of the elasticity of polymer melt in linear steady flow, it is expected that there exists a correlation between ν and J_e^0. However, no correlation was found between them. There was a weak correlation between ν and η_{0p} which is a measure of the viscosity in linear steady flow. But there existed a good correlation between log ν and log $(\eta_{0p}^2 \cdot J_e^0)$ as shown in Figure 10. Thus, the following equation was obtained:

$$\log \nu \propto \log (\eta_{0p}^2 \cdot J_e^0). \tag{19}$$

The symbol $\propto$ employed in this paper means that there is a positive correlation between the left and the right sides. $\eta_{0p}^2 \cdot J_e^0$ equals to the elasticity coefficient A_G, defined by the following equation:

$$A_G = \lim_{\dot{\gamma} \to 0} \frac{(\sigma_{11} - \sigma_{22})}{2\dot{\gamma}^2} \tag{20}$$

where $(\sigma_{11} - \sigma_{22})$ is the first normal stress difference and $\dot{\gamma}$ is the shear rate. Physical meaning of $\eta_{0p}^2 \cdot Je^0$ is a measure of stored energy in linear steady flow. It is of great interest that there is a positive correlation between ν and $\eta_{0p}^2 \cdot J_e^0$, which are a measure of the elasticity of nonlinear steady flow and a measure of the stored energy in linear steady flow, respectively. As η_{0p} is governed mainly by weight-average molecular weight and J_e^0 is governed mainly by molecular weight distribution,[19,20] it is assumed that ν is governed by both molecular weight and molecular weight distribution. This assumption is supported by the experimental result of Kamide et al.[18]

The ν values shown in Figure 10 are limited to shear rates from 10^2 sec^{-1} to 10^3 sec^{-1}. This is why, since the flow curve of the sample with high M.I. cannot be measured at the shear rate below 10^2 sec^{-1} by means of a die with a small L/R value, as mentioned before, the Bagley plot was done by

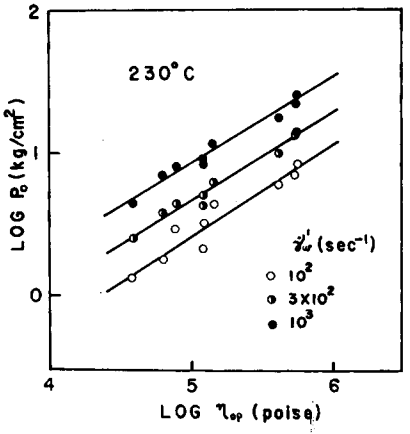

Fig. 12. Relation between P_0 and η_{0p}.

extrapolation and hence the reliability of the ν value is low at a shear rate below 10^2 sec^{-1}. On the other hand, since the apparent flow curves of the sample with high M.I. crease at a shear rate just above 10^3 sec^{-1}, as shown in Figure 8, and melt fracture occurs at a shear rate just above 10^3 sec^{-1} for the sample with low M.I., the possibility of a change in flow mechanism is high at a shear rate above 10^3 sec^{-1}.

The pressure loss at die inlet P_0, which is obtained as the intercept of the P axis of a Bagley plot, is plotted against the apparent shear rate $\dot{\gamma}_w'$ in Figure 11. As shown in Figure 12, P_0 correlated well with η_{0p} as follows:

$$\log P_0 \propto \log \eta_{0p} \tag{21}$$

Here, the shear rate was also limited to 10^2 sec^{-1} to 10^3 sec^{-1} for the same reason as mentioned before.

Bogue[21] studied minutely the pressure loss at the inlet of a capillary in non-Newtonian flow. According to his results, P_c in eq. (10) is negligible in comparison with P_e over the shear rate range of this study, and hence

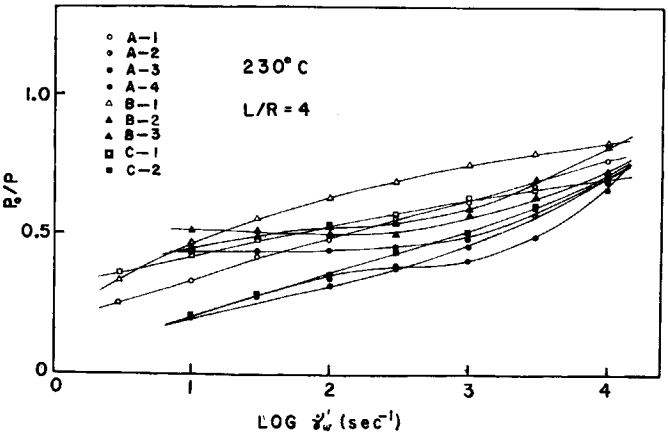

Fig. 13. Shear rate variation of elastic pressure loss ratio P_0/P.

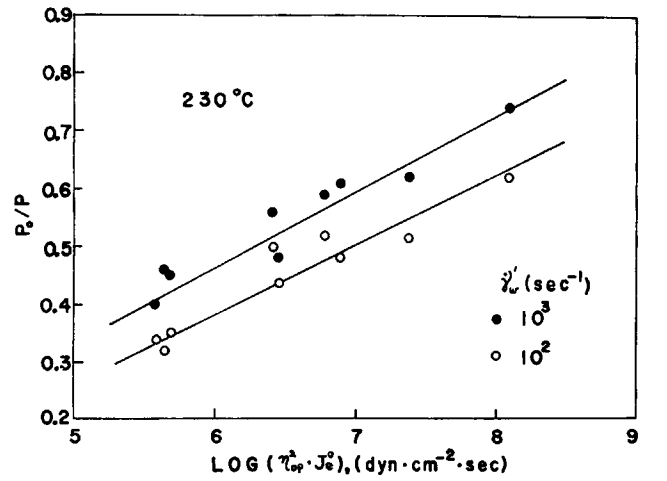

Fig. 14. Relation between P_0/P and $\eta^2_{0p} \cdot J_e^0$

$P_0 \fallingdotseq P_e$. Philippoff[28] also obtained the same experimental results. Consequently, P_0 is regarded as the elastic pressure loss.

As it is expected that when the elastic pressure loss is large, the viscous pressure loss is also large, the elastic pressure loss ratio and the viscous pressure loss ratio were defined as P_0/P and $1 - (P_0/P)$, respectively, where P was the whole pressure loss. The relative strengths of elasticity and viscosity of a polymer melt in capillary flow were evaluated by P_0/P and $1 - (P_0/P)$. As the whole pressure loss P increases with L/R at a constant shear rate, the elastic pressure loss ratio P_0/P decreases with L/R. The P_0/P values in the case of $L/R = 4$ are plotted against the apparent shear rate $\dot{\gamma}_w'$ in Figure 13. As P_0/P increased with increase in shear rate, the elasticity of polypropylene melt increased with the increase in shear rate.

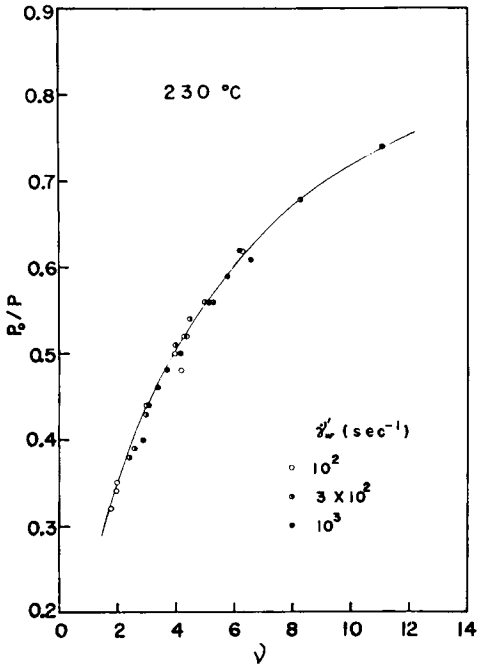

Fig. 15. Relation between elastic pressure loss ratio P_0/P and end correction coefficient ν.

There was no correlation between the elastic pressure loss ratio P_0/P and J_e^0, and there was a weak correlation between P_0/P and η_{0p}. There existed a good correlation between P_0/P and log $(\eta_{0p}^2 \cdot J_e^0)$ as shown in Figure 14. Thus, the following equation was obtained:

$$P_0/P \propto \log (\eta_{0p}^2 \cdot J_e^0). \tag{22}$$

It was assumed that, as in the case of ν, P_0/P also became larger with increase in the weight-average molecular weight and with increase in the molecular weight distribution.

Though both the end correction coefficient ν and the elastic pressure loss ratio P_0/P are a measure of the elasticity of polymer melt in capillary flow, P_0/P has a clearer physical meaning than ν from the viewpoint of a measure of elasticity. Figure 15 shows that there is a very close relation between P_0/P and ν. This fact is understandable from eq. (23), rearranged from eq. (9′):

$$P_0/P = \frac{\nu R}{(L + \nu R)}. \tag{23}$$

Flow Curve

The apparent flow curves in the form of $\dot{\gamma}_w'$ versus τ_w' and $\dot{\gamma}_w'$ versus τ, and the true flow curve in the form of $\dot{\gamma}$ versus τ are shown together in

Figure 6. When the apparent shear stress τ_w' was end-corrected to the effective shear stress τ, each flow curve with different L/R united into one curve independent of L/R. Although the apparent flow curves in the form of $\dot{\gamma}_w'$ versus τ_w' for the sample with high M.I. had creases at the shear rate of about 10^3 sec^{-1}, as shown for the A-3 sample in Figure 8, these creases vanished when τ_w' was corrected to τ.

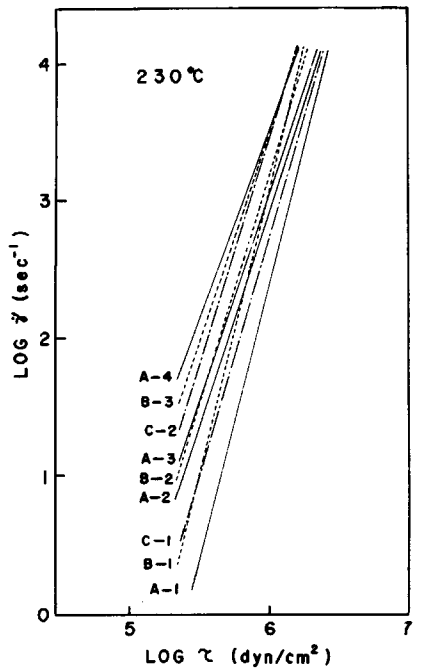

Fig. 16. True flow curves for all samples.

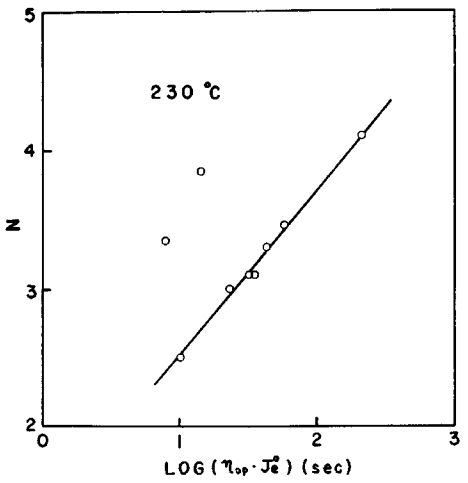

Fig. 17. Relation between power law index N and $\eta_{0p} \cdot J_e^0$

The true flow curves of all samples are collected in Figure 16. All flow curves were linear when log $\dot{\gamma}$ was plotted against log τ. Thus, the so-called power law held:

$$\dot{\gamma} = K\tau^N \tag{24}$$

where K and N are constants; N is a measure of non-Newtonianity in steady flow and is called the power law index. Since after Dexter[22] the clasticity of a polymer melt is a component of non-Newtonianity in steady flow of a polymer melt, it is expected that there exists a correlation between N and J_e^0 which is a measure of elasticity in linear steady flow. However, there was no correlation between them. Meanwhile, there was a considerably good correlation between N and η_{0p}. Furthermore, as shown in Figure 17, there was a very good correlation between N and log $(\eta_{0p} \cdot J_e^0)$ through there were two unusual values. Thus, the following equation was obtained:

$$N \propto \log (\eta_{0p} \cdot J_e^0). \tag{25}$$

Consequently, it was assumed that non-Newtonianity became stronger with increase in the weight-average molecular weight and with increase in the molecular weight distribution. This assumption is supported by the experimental result of Kamide et al.[23] The physical meaning of $\eta_{0p} \cdot J_e^0$ is the mean relaxation time.

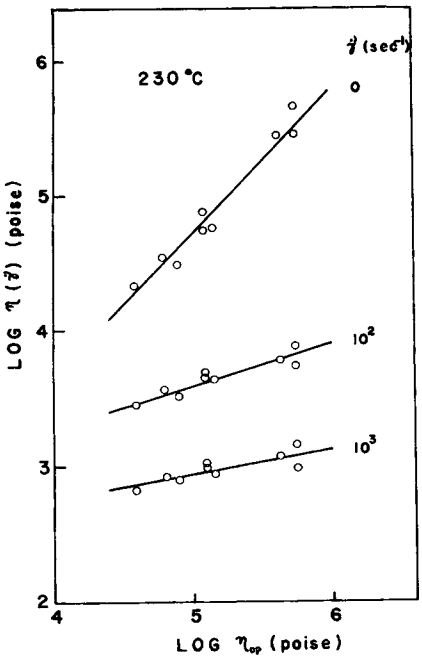

Fig. 18. Relation between steady flow viscosity η and η_{0p}.

Steady Flow Viscosity

The apparent viscosity η, calculated by use of eq. (15) from the true flow curve in Figure 17, is plotted against η_{0p} in Figure 18. η correlated very well with η_{0p} as follows:

$$\log \eta \propto \log \eta_{0p}. \tag{26}$$

The correlation coefficient of log η versus log η_{0p} decreased with increase in shear rate. Meanwhile, as log η_{0p} correlated with log $\bar{M}_v$, as shown in Figure 5, log η also correlates with log $\bar{M}_v$. Consequently, $\bar{M}_v$ dependency of η decreases with increase in shear rate. This tendency agrees with the experimental results of Schreiber et al.[24] and Kamide et al.[23] The zero-shear viscosity η_0 was obtained by means of the procedure of Kamide et al.[20] When $1/\log \eta$ was plotted against shear stress τ, a linear relationship was obtained, and η_0 could be obtained from the intercept of the straight line by extrapolating τ to 0. The slope of log η_0 versus log η_{0p} was about 1, and hence η_0 was nearly proportional to η_{0p}. But the absolute value of η_0 was about half that of η_{0p}.

Barus Effect

It is well known that when a viscoelastic fluid such as polymer melt is extruded through a capillary, the extrudate swells to a larger diameter than that of the capillary. This phenomenon is called Barus effect or Merrington effect. Although there are many explanations[25] for the Barus effect, in any event it can be said that the Barus effect originates in the elasticity of the polymer melt.

After the extrudate solidified, the diameter of the extrudate, D, was measured with a micrometer. The ratio D/D_0, where D_0 is the diameter of the capillary, was defined as the swelling ratio and was used as a measure of the Barus effect. In measuring D, the extrudate was cut off when it was short and was laid and cooled to eliminate the draw-down effect. It was

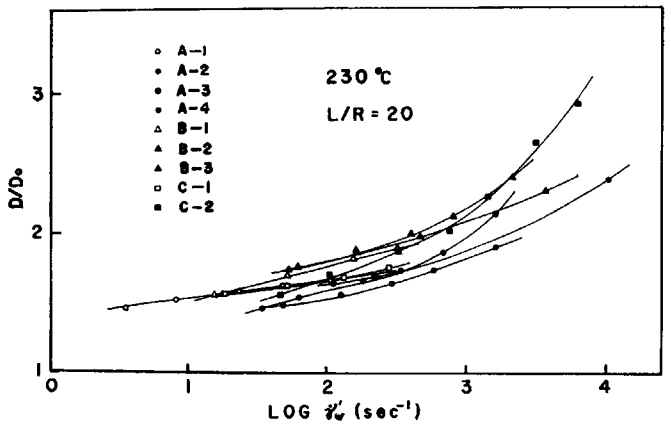

Fig. 19. Shear rate variation of swelling ratio D/D_0.

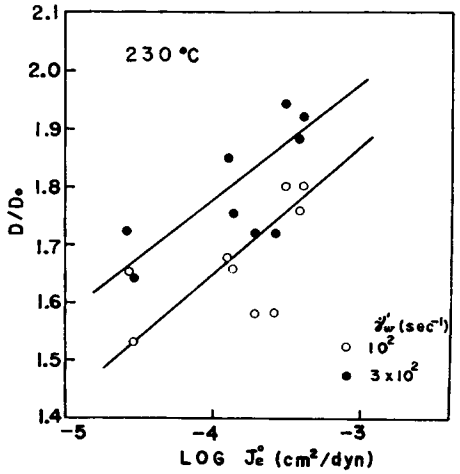

Fig. 20. Relation between D/D_0 and J_e^0

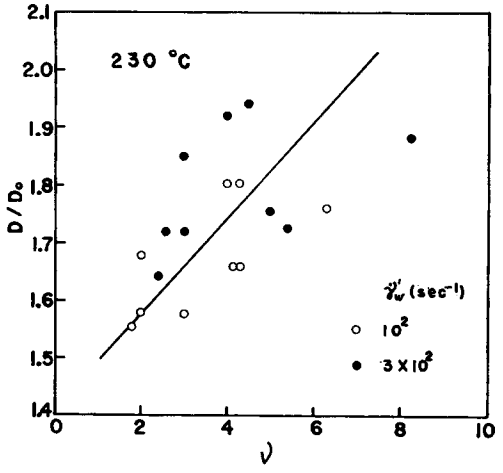

Fig. 21. Relation between swelling ratio D/D_0 and end correction coefficient ν.

observed that the smaller the L/R value of the die, the larger the D/D_0 value was. When L/R was small, since we could not obtain the extrudats at low shear rate for samples with high M.I. on account of the lower limit of applied pressure in the Koka flow tester, and since melt fracture occurred at low shear rate for the sample with low M.I. and hence D could not be measured, there was no shear rate range where the D/D_0-versus-shear rate curves for all samples could be superimposed. Consequently, in order that D/D_0-versus-shear rate curves for all samples could be superimposed in as broad a shear rate range as possible, D/D_0 was measured for the extrudate obtained from the die having the largest L/R ($=20$). D/D_0 is shown against the apparent shear rate $\dot{\gamma}_w'$ in Figure 19; D/D_0 increased with increase in shear rate.

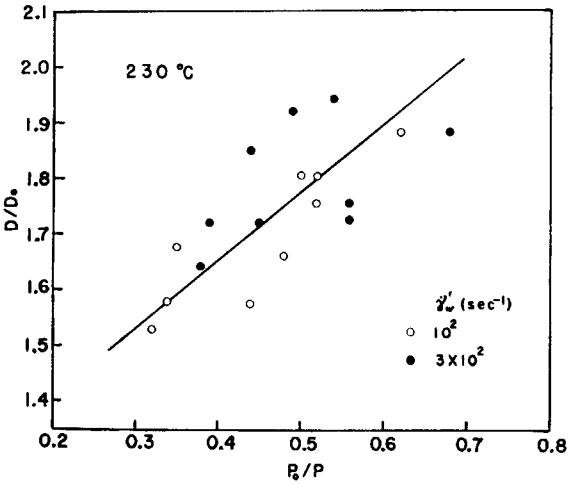

Fig. 22. Relation between swelling ratio D/D_0 and elastic pressure loss ratio P_0/P.

Over the shear rate range from 10^2 sec^{-1} to 3×10^2 sec^{-1} where D/D_0-versus-$\dot{\gamma}_w'$ curves of all samples superimposed, there was almost no correlation between D/D_0 and η_{0p}, but there was a positive correlation between D/D_0 and J_e^0 as shown in Figure 20. Accordingly, the higher J_e^0 or the broader the molecular weight distribution, the more pronounced the Barus effect is. If the Barus effect can be defined such that when polymer melt flows from the reservoir with a relatively large diameter into a capillary with relatively small diameter, an elastic deformation is given to the polymer melt, and the elastic deformation recovers at the exit of the capillary, then it can be assumed that Barus effect is significant with easily deformable material. Since J_e^0 is a measure of the ease of elastic deformation of polymer melt in steady flow, it is expected that the higher J_e^0, the more notable the Barus effect is. This expectation agrees with the experimental result. However, the steady-state compliance J_e^0 employed here is in linear steady flow. Though the steady-state compliance J_e in nonlinear steady flow decreases with the increase in shear rate,[26] it was assumed that the order of largeness did not change. As the end correlation coefficient is a measure of the elasticity of polymer melt, the Barus effect also reflects the elasticity of the polymer melt. Hence it is expected that there is a positive correlation between them. As expected, there was a positive correlation between the swelling ratio D/D_0 and the end correction coefficient ν as shown in Figure 21. There was also a positive correlation between D/D_0 and the elastic pressure loss ratio P_0/P, which was also a measure of the elasticity of polymer melt, as shown in Figure 22; D/D_0 showed better correlation with P_0/P than with ν.

Melt Fracture

When polymer melt is extruded through a capillary, the extrudate shows a helical or irregular shape at high shear rate or shear stress. This phe-

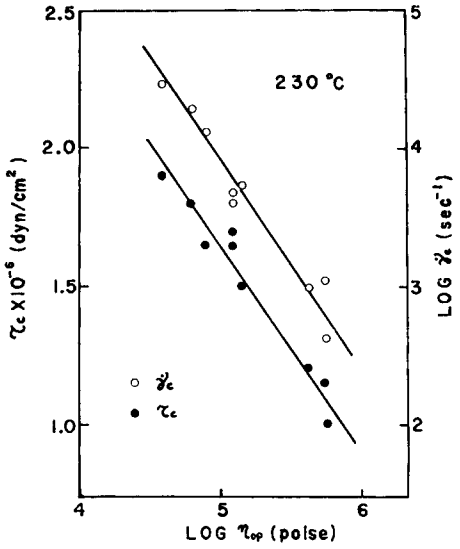

Fig. 23. Relations between critical shear stress τ_c and critical shear rate γ_c and η_{0p}.

nomenon is called melt fracture and is considered to originate in the elasticity of polymer melt.

Melt fracture begins to occur at the closed points in the flow curves in Figure 6. The apparent critical shear stress τ_{wc} at which the melt fracture begins to occur varied with the L/R of the die. However, when the apparent shear stress τ_w' was end-corrected to the effective shear stress τ, the critical shear stress τ_c was nearly constant independently of the dimensions of the die. Average τ_c's obtained from the five kinds of dies are plotted against η_{0p} in Figure 23. τ_c had a very good correlationship with η_{0p} as follows:

$$\tau_c \propto -\log \eta_{0p} \tag{27}$$

Since η_{0p} increased with increase in $\bar{M}_v$ as shown in Figure 5, τ_c must decrease with increase in $\bar{M}_v$. This disagreed with the experimental result for the fractions of polypropylene by Kamide et al.[22] in which τ_c was independent of molecular weight. The product $\tau_c \cdot \bar{M}_v$ for each sample is shown in Figure 24, where the samples on the abscissa are arranged so that $\bar{M}_v$ becomes higher going to the right. $\tau_c \cdot \bar{M}_v$ was nearly constant (4.5×10^{11} dyne/cm^2) independently of molecular weight. This tendency agreed with the experimental result of Spencer and Dillon.[27] The critical shear rate $\dot{\gamma}_c$ is also plotted against η_{0p} in Figure 23; $\dot{\gamma}_c$ correlated very well with η_{0p} as follows:

$$\log \dot{\gamma}_c \propto -\log \eta_{0p}. \tag{28}$$

It was assumed from eqs. (27) and (28) that the critical shear stress τ_c and the critical shear rate $\dot{\gamma}_c$ were governed mainly by the weight-average

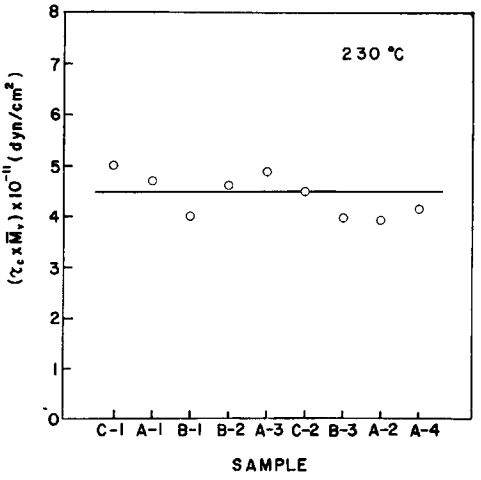

Fig. 24. Dependence of $\tau_c \cdot \bar{M}_v$ on $\bar{M}_v$.

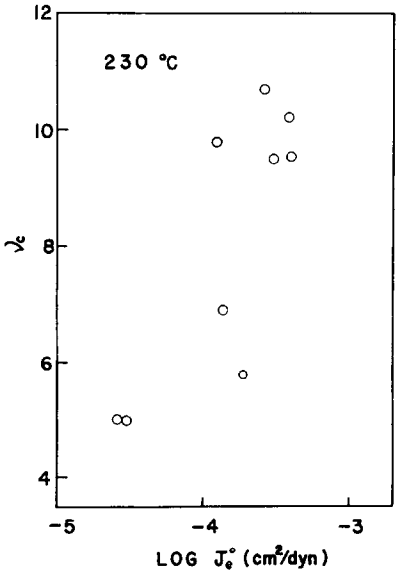

Fig. 25. Relation between critical end correction coefficient ν_c and J_e^0.

molecular weight and were almost unaffected by the molecular weight distribution.

The end correction coefficient ν_c at the critical shear rate $\dot{\gamma}_{wc}$ is plotted against J_e^0 in Figure 25. There was a weak positive correlation between ν_c and J_e^0. Philippoff and Gaskins[28] derived the following equation:

$$\nu = n_c + S_R/2 \tag{29}$$

where ν is the end correction coefficient, n_c is the Couette's correction term coefficient, and S_R is the recoverable shear strain. It can be considered

that this equation holds at the critical state at which the melt fracture begins to occur, and n_c whose value is about 0.77[13] is negligible in comparison with ν_c. Hence, eq. (29) becomes

$$S_{Rc} = 2\nu_c. \tag{30}$$

It was seen from Figure 25 and eq. (30) that the critical recoverable shear strain S_{Rc} for polypropylene ranged from about 10 to 20 and increased with the increase in J_e^0. Tordella[29] experimentally obtained an S_{Rc} value of about 5, independently of the kind of polymer. But in this study, had the sample been restricted to only polypropylene, the value of S_{Rc} ranged from about 10 to 20, hence was considerably larger than that of Tordella and varied with J_e^0.

CONCLUSIONS

1. By representing the linear viscoelasticity numerically with the zero-shear viscosity η_{0p} and the steady-state compliance J_e^0, evaluation was made of the properties concerning the elasticity of polymer melt in capillary flow, such as non-Newtonianity, entrance pressure loss, end correction, Barus effect, and melt fracture.

2. η_{0p} measured with a plate relaxometer correlated with the viscosity-average molecular weight $\bar{M}_v$ as follows:

$$\eta_{0p} \propto \bar{M}_v^{4.0}.$$

3. The end correction coefficient ν correlated with η_{0p} and J_e^0 as follows:

$$\log \nu \propto \log (\eta_{0p}^2 \cdot J_e^0)$$

and hence it was assumed that ν was governed by both the molecular weight and the molecular weight distribution. $\eta_{0p}^2 \cdot J_e^0$ equals the elastic coefficient A_G and is a measure of the stored energy in linear steady flow.

4. The entrance pressure loss P_0 correlated with η_{0p} as follows:

$$\log P_0 \propto \log \eta_{0p}$$

and hence it was assumed that P_0 was governed mainly by molecular weight.

5. The elastic pressure loss ratio P_0/P correlated with η_{0p} and J_e^0 as follows:

$$P_0/P \propto \log (\eta_{0p}^2 \cdot J_e^0)$$

and hence it was assumed that P_0/P was governed by both molecular weight and molecular weight distribution.

6. The true flow curves were straight lines over the shear rate range from 10 sec^{-1} to 10^4 sec^{-1} when $\log \dot{\gamma}$ was plotted against $\log \tau$, and thus the so-called power law held. The power law index N correlated with η_{0p} and J_e^0 as follows:

$$N \propto \log (\eta_{0p} \cdot J_e^0)$$

and hence it was assumed that N was governed by both molecular weight and molecular weight distribution. The physical meaning of $\eta_{0p} \cdot J_e^0$ is the mean relaxation time.

7. The steady flow viscosity η measured with a capillary viscometer correlated with η_{0p} as follows:

$$\log \eta \propto \log \eta_{0p}.$$

The correlation coefficient decreased with increase in shear rate. The zero-shear viscosity η_0 was proportional to η_{0p}. However, the absolute value of η_0 was about half that of η_{0p}.

8. The swelling ratio D/D_0, which is a measure of the Barus effect, had positive correlationships with J_e^0, ν, and P_0/P.

9. The critical shear stress τ_c and the critical shear rate $\dot{\gamma}_c$ at which melt fracture begins to occur correlated with η_{0p} as follows:

$$\tau_c \propto -\log \eta_{0p}$$

$$\log \dot{\gamma}_c \propto -\log \eta_{0p}$$

and hence τ_c and $\dot{\gamma}_c$ were governed mainly by molecular weight. The following equation was obtained:

$$\tau_c \cdot \bar{M}_v = \text{const.} \ (= 4.5 \times 10^{11}).$$

10. The critical recoverable shear strain S_{Rc} ranged from 10 to 20 and had a positive correlationship with J_e^0.

The authors would like to thank Professor M. Takayanagi of Kyushu University for his encouragement during this work and the Tokuyama Soda Co., Ltd., for permission to publish this paper.

References

1. B. D. Coleman and H. Markovitz, Jr., *J. Appl. Phys.*, **35**, 1 (1964).
2. Y. H. Pao, *J. Appl. Phys.*, **28**, 591 (1957).
3. Y. H. Pao, *J. Polym. Sci.*, **61**, 413 (1962).
4. Y. H. Pao, *J. Polym. Sci. B*, **2**, 437 (1964).
5. T. W. Huseby and L. L. Blyler, Jr., *Trans. Soc. Rheol.*, **11**, 77 (1967).
6. W. P. Cox and E. H. Merz, *J. Polym. Sci.*, **28**, 619 (1958).
7. W. P. Cox and E. H. Merz, *Special Technical Publication of A.S.T.M.* No. 247 1958, p. 178.
8. W. P. Cox, *Official Digest of the Federation of Societies for Paint Technology*, May 1960, p. 2.
9. S. Onogi, T. Fujii, H. Kato, and S. Ogiwara, *J. Phys. Chem.*, **68**, 1598 (1964).
10. P. Parrini, F. Sebastiano, and G. Messina, *Makromol. Chem.*, **38**, 27 (1960).
11. M. Fujiyama, S. Uemura, and M. Takayanagi, *Kogyo Kagaku Zasshi*, **71**, 540 (1968).
12. J. D. Ferry, *Viscoelastic Properties of Polymers*, Interscience, New York, 1962.
13. S. Iwanami, *Trans. Japan Soc. Mech. Eng.*, **18**, 52, 59 (1952).
14. I. M. Krieger and S. H. Maron, *J. Appl. Phys.*, **23**, 147 (1952).
15. E. B. Bagley, *J. Appl. Phys.*, **28**, 624 (1957).
16. T. G. Fox and S. Loshak, *J. Appl. Phys.*, **26**, 1081 (1955).
17. K. Kamide, Y. Inamoto, and K. Ono, *Kobunshi Kagaku*, **22**, 410 (1965).

18. K. Kamide and K. Fujii, *Kobunshi Kagaku*, **24**, 120 (1967).
19. H. J. M. A. Mieras and C. F. H. van Rizin, *Nature*, **218**, 865 (1968).
20. N. J. Mills, *Eur. Polym. J.*, **5**, 675 (1969).
21. D. C. Bogue, *Ind. Eng. Chem.*, **51**, 874 (1959).
22. F. D. Dexter, *J. Appl. Phys.*, **25**, 1124 (1954).
23. K. Kamide, Y. Inamoto, and K. Ono, *Kobunshi Kagaku*, **22**, 529 (1965).
24. H. P. Schreiber, E. B. Bagley, and D. C. West, *Polymer*, **4**, 355 (1963).
25. K. Kamide, Y. Inamoto, and K. Ono, *Kobunshi Kagaku*, **22**, 505 (1965).
26. T. Kataoka, *J. Appl. Polym. Sci.*, **12**, 1009 (1968).
27. R. S. Spencer and R. E. Dillon, *J. Colloid Sci.*, **3**, 163 (1948); *ibid.*, **4**, 241 (1949).
28. W. Philippoff and F. H. Gaskins, *Trans. Soc. Rheol.*, **2**, 263 (1958).
29. J. P. Tordella, *J. Appl. Polym. Sci.*, **7**, 215 (1963).
30. H. L. La Nieve, III, and D. C. Bogue, *J. Appl. Polym. Sci.*, **12**, 353 (1968).

Received August 19, 1971
Revised September 17, 1971